Journal of CO_2 Utilization 22 (2017) 71–80

Contents lists available at ScienceDirect

Journal of CO_2 Utilization

journal homepage: www.elsevier.com/locate/jcou

Optimization of the Pd/Cu ratio in Pd-Cu-Zn/SiC catalysts for the CO_2 hydrogenation to methanol at atmospheric pressure

J. Díez-Ramírez*, J.A. Díaz, P. Sánchez, F. Dorado

Departamento de Ingeniería Química, Facultad de Ciencias y Tecnologías Químicas, Universidad de Castilla – La Mancha, Avenida Camilo José Cela 12, 13071 Ciudad Real, Spain

ARTICLE INFO

Keywords:
CO_2 hydrogenation
Methanol synthesis
Trimetallic catalysts
Pd-Cu-Zn
Silicon carbide
Atmospheric pressure

ABSTRACT

PdCuZn/SiC catalysts were synthesized with different Pd:Cu:Zn molar compositions and tested in the hydrogenation of carbon dioxide to methanol at atmospheric pressure. Trimetallic catalysts were compared with the corresponding bimetallic ones (PdZn/SiC, CuZn/SiC and PdCu/SiC). Catalysts were characterized by N_2 adsorption/desorption, temperature-programed reduction (TPR), X-ray diffraction (XRD), transmission electron microscopy (TEM), energy dispersive X-ray spectroscopy (EDS) and X-ray photoelectron spectroscopy (XPS). The Pd^0 active sites were related to carbon monoxide formation via reverse water-gas-shift (RWGS), whereas the PdZn alloys catalyzed methanol synthesis. The role of copper in trimetallic catalysts was to inhibit the deposition of metallic palladium by forming a PdCu alloy that proved to be less active to CO formation. Moreover, the active sites of trimetallic catalysts were smaller and better dispersed than those of the corresponding bimetallic ones, probably due to a synergistic effect between the three metals. The catalyst with a molar composition of 37.5:12.5:50 Pd:Cu:Zn (mol.%) was selected as the most active for the methanol synthesis, as this sample showed the highest activity and selectivity to methanol. The role of copper was also shown to be crucial in trimetallic catalyst by comparing the best example with an equivalent bimetallic PdZn/SiC with a Pd:Zn molar ratio of 37.5:62.5.

1. Introduction

Carbon dioxide emissions not only lead to dramatic environmental problems, from their contribution to global warming [1] to acidification of the oceans [2], but also to important economic issues [3]. The development of new legislation concerning CO_2 emissions and the challenging targets set by the global Paris Agreement and the EU 2030 Framework for Climate and Energy are forcing governments and companies to implement innovative solutions to prevent and reduce CO_2 emissions [4].

In this sense, the valorization of CO_2 has gained attention in recent decades [5–9] since it provides both a reduction of atmospheric emissions and the synthesis of added-value chemicals. In this respect, the hydrogenation of CO_2 (Eq. (1)) has been assessed as one of the potential valorization routes, from which CO, hydrocarbons, alcohols or aldehydes can be produced [6,8].

$$xCO_2 + (2x - z + y/2)\ H_2 \rightarrow C_xH_yO_z + (2x - z)\ H_2O \quad (1)$$

Methanol is reported to be one of the most interesting products (Eq. (2)) because it is used as a solvent and a feedstock for the production of chemicals [7,10]. Furthermore, methanol could be used as an alternative fuel in the energy distribution infrastructure that currently exists or it could be blended with gasoline [11]. The economic limitation of this reaction is currently related to the use of high amounts of hydrogen in the process, which could be overcome by applying different technologies such as the electrolysis of water using renewable energies (e.g., solar energy) [12].

$$CO_2 + 3H_2 \leftrightarrows CH_3OH + H_2O \quad \Delta H_{25°C} = -49.5\text{kJ/mol} \quad (2)$$

Due to the stable nature of the CO_2 molecule, this reaction needs to overcome a high thermodynamic barrier. CO_2 activation takes place at 150–200 °C and at this temperature the reverse WGS reaction (Eq. (3)), which has an adverse effect on methanol production, also occurs.

$$CO_2 + H_2 \leftrightarrows CO + H_2O \quad \Delta H_{25°C} = 41\text{kJ/mol} \quad (3)$$

Therefore, the use of catalysts to control the selectivity towards the different products is a prerequisite. Although metals such as Au [13–15], Ag [16] or Mo [17] have been used in CO_2 hydrogenation to methanol, copper- and palladium-based catalysts have been the most widely studied because of their well-known properties and high efficiency in this reaction [18–24]. Indeed, the bimetallic Pd-Cu

* Corresponding author.
E-mail address: Javier.Diez@uclm.es (J. Díez-Ramírez).

http://dx.doi.org/10.1016/j.jcou.2017.09.012
Received 24 June 2017; Received in revised form 25 August 2017; Accepted 15 September 2017
Available online 25 September 2017

Table 1
Nomenclature and main physical properties of the catalysts.

Nomenclature	Metal loading (mol.%)						Surface area ($m^2 g^{-1}$)	Total pore volume x 10^2 ($cm^3 g^{-1}$)	Average pore radius (nm)	XRD – Particle diameter (nm)[a]	TEM – Particle diameter (nm)
	Palladium		Copper		Zinc						
	Theo.	Exp.	Theo.	Exp.	Theo.	Exp.					
SiC	–	–	–	–	–	–	25	14.1	11.5	–	–
CuZn/SiC	–	–	50	54	50	46	17	10.7	12.5	52 (Cu)	40.2
PdZn/SiC	50	55	–	–	50	45	29	11.7	8.0	22 (PdZn)	20.0
PdCu/SiC	50	40.7	50	59.3	–	–	25	16.8	13.4	53 (PdCu) 50 (Cu)	28.5
12.5PdCuZn/SiC	12.5	16	37.5	40	50	44	21	13.4	13.0	26 (PdCuZn) 35 (Cu)	25.6
25PdCuZn/SiC	25	30	25	24	50	46	23	13.4	11.5	14 (PdCuZn)	–
37.5PdCuZn/SiC	37.5	39.4	12.5	14.3	50	46.3	29	12.5	8.4	11 (PdCuZn)	12.5

[a] In brackets, the compound which it refers to.

configuration has also been studied at high pressure and the main conclusion was that the PdCu alloy formed was a crucial factor for the bimetallic promotion [25]. On the other hand, zinc oxide (ZnO) has been reported to enhance the catalytic performance of Cu and Pd. In the case of Pd, ZnO is necessary to form the PdZn alloy, which has proven to be more active and selective to methanol than the corresponding isolated metals [22,24]. Regarding Cu catalysts, Ahouari et al. [18] summarized the role of ZnO as follows: (i) it promotes higher dispersion of Cu, thus preventing the agglomeration of Cu particles, (ii) it improves the resistance of Cu particles to poisoning by feed gas impurities, (iii) ZnO, as a basic oxide, partially neutralizes the acidity of the catalyst and enhances CO_2 adsorption on the catalyst surface and (iv) ZnO also acts as a reservoir of atomic hydrogen and provides this gas to achieve methanol synthesis on the Cu surface.

The combination of these three metals has been reported previously in the literature [26–29]. Melían-Cabrera et al. [27] compared CuO/ZnO with Pd-promoted CuO/ZnO catalysts (PdO:CuO:ZnO = 2:28:70 wt.%) under an operating pressure of 60 bar and found a considerable improvement when Pd was used. They suggested that this improvement was a result of an enhancement of the spillover mechanism of H_2 due to the presence of Pd, as well as a further stabilization of Cu due to possible PdCu alloy formation. More recently, Siriworarat et al. [29] studied the influence of Pd loading (5, 10 and 15 wt.%) on a Pd-Cu-Zn catalyst in which Cu and Zn were settled at 25 wt.%. In this study, which was carried out at 250 °C and 25 bar, the highest performance was observed on using the catalyst containing 15 wt.% Pd, 25 wt.% Cu and 25 wt.% Zn, which gave methanol selectivity and space time yield of 25% and 112 g kg cat^{-1} h^{-1}, respectively. Although these papers revealed that the combination of these metals improves the methanol yield, they only considered the role of Pd as a promoter of Cu/Zn catalysts and did not obtain an optimum composition for the catalyst. As Pd is reported to be active in this reaction, an in-depth study on the Pd-Cu-Zn composition is still necessary.

Regarding supports, different materials have been used to date (Al_2O_3, CeO_2, SiO_2, ZrO_2, CNF, CNT, etc.) [22,30–36]. However, the use of β-SiC in this reaction has not been widely reported in the literature [37], even though it has shown excellent properties in many reactions [38–43]. β-SiC exhibits high thermal conductivity and mechanical strength, low specific weight and chemical inertness, so that this support is appropriate to avoid interactions with the active phases.

In the work reported here trimetallic Pd-Cu-Zn catalysts were prepared, characterized and tested in the synthesis of methanol from CO_2 hydrogenation at atmospheric pressure. Taking into account the secondary role of Zn in Pd/ZnO and Cu/ZnO formulations (see above), a highly enough proportion of Zn was deposited in each catalyst. On the other hand, as Pd and Cu are reported to be the active phases in these formulations, the proportion of these metals was modified in a broad range in order to get an optimal trimetallic formulation. These catalysts were compared with the corresponding bimetallic ones (PdCu, PdZn and CuZn). In all cases, β-SiC was used as a support. To the best of our knowledge, there is a lack of studies that deal with this reaction at atmospheric pressure [21,22,24,44,45].

2. Experimental

2.1. Catalyst preparation

Catalysts were prepared by the impregnation method using β-SiC (SICAT CATALYST, pellets) as support and three different nitrates as precursors of the Cu, Pd and Zn: copper(II) nitrate trihydrate [$Cu(NO_3)_2{\cdot}3H_2O$, Panreac, 99.95% purity], palladium(II) nitrate [$Pd(NO_3)_2{\cdot}xH_2O$, Aldrich] and zinc nitrate hexahydrate [$Zn(NO_3)_2{\cdot}6H_2O$, Panreac, 99% purity].

Firstly, 5 g of the support were placed in a glass vessel and kept under vacuum at room temperature (~25 °C) for 2 h to remove water and other impurities adsorbed on the structure. Secondly, an aqueous solutions of the corresponding metal nitrates were poured over the support, using the appropriate quantities to obtain catalysts with a total amount of 0.01 mol and different Pd, Cu and Zn contents, as shown in Table 1. Thirdly, the solvent was removed under vacuum at 90 °C for 2 h. After impregnation, the catalysts were dried at 120 °C overnight.

The calcination was carried out at 500 °C in a Nabertherm HTC 03/15 furnace, which was open to the atmosphere. This temperature was kept constant for 3 h and the heating rate was 5 °C min^{-1}. Prior to the reaction, the catalysts were reduced in situ in a 25% v/v H_2/N_2 stream at a flow rate of 100 Ncm^3 min^{-1} from room temperature to 500 °C with a heating rate of 1.3 °C min^{-1}.

The nomenclature of the catalysts is shown in Table 1. Trimetallic catalysts are denoted as XPdCuZn/SiC, where X indicates the theoretical molar percentage of metallic palladium in the sample.

2.2. Support/catalyst characterization

The Cu, Pd and Zn metal loadings were determined by atomic absorption (AA) spectrophotometry on a SPECTRA 220FS analyzer. Samples (*ca.* 0.5 g) were treated with 2 mL HCl, 3 mL HF and 2 mL H_2O_2 followed by microwave digestion (250 °C). Surface area/porosity measurements were carried out on a QUADRASORB 3SI sorptometer apparatus with N_2 as the sorbate at −196 °C. The samples were outgassed at 250 °C under vacuum (5×10^{-3} Torr) for 12 h prior to analysis. Specific surface areas were determined by the multi-point BET method and the mesopore size distribution with the BJH method. Specific total pore volume was evaluated from N_2 uptake at a relative pressure of $P/P_0 = 0.99$. The relative error of the all the experiments was ± 5% Temperature-programed reduction (TPR) experiments were conducted in a commercial Micromeritics AutoChem 2950 HP unit with TCD detection. Samples (*ca.* 0.15 g) were loaded into a U-shaped tube and ramped from room temperature (~25 °C) to 900 °C (10 °C min^{-1}), with a reducing gas mixture of 20% v/v H_2/Ar (60 cm^3 min^{-1}). XRD experiments were conducted on a Philips X'Pert instrument using

nickel-filtered Cu-Kα radiation. Samples were scanned at a rate of 0.02° $step^{-1}$ over the range 5° ≤ 2θ ≤ 90° (scan time = 2 s $step^{-1}$). Transmission electron microscopy (TEM) analyses were carried out on a JEOL JEM-4000EX unit with an accelerating voltage of 400 kV. Samples were prepared by ultrasonic dispersion in acetone with a drop of the resulting suspension evaporated onto a holey carbon-supported grid. The instrument was equipped with an energy dispersive X-ray spectroscopy (EDS) unit. Saturation was assumed to be complete after three successive peaks showed the same peak areas.

The particle size was calculated from TEM images. The mean particle size evaluated as the surface-area weighted diameter (d_s) was computed according to:

$$\bar{d}_s = \frac{\sum_i n_i d_i^3}{\sum_i n_i d_i^2} \quad (4)$$

where n_i represents the number of particles with diameter d_i ($\Sigma_i n_i \geq 200$).

XPS analyses were performed on an ESCAPlus Omicron spectrometer using a monochromatized Mg source (MnKα 1253.6 eV). The high-resolution spectra were recorded with a 40 eV pass energy, and the constant charging of the samples was corrected by referencing all energies to the C_{1s} peak at 284.6 eV. Curve fitting was performed using the CasaXPS software.

2.3. Catalyst activity

Catalytic performance tests were carried out in a tubular quartz reactor (45 cm length and 1 cm diameter). The catalyst, which consisted of pellets that were 3 mm length and 1 mm diameter, was placed on a fritted quartz plate located at the end of the reactor. The amount of catalyst used in the experiments was 0.8 g.

The temperature of the catalyst was measured with a K-type thermocouple (Thermocoax) placed inside the inner quartz tube. The entire reactor was placed in a furnace (Lenton) equipped with a temperature-programed system. Reaction gases were Praxair certified standards of CO_2 (99.999% purity), H_2 (99.999% purity) and N_2 (99.999% purity). The gas flows were controlled by a set of calibrated mass flowmeters (Brooks 5850 E and 5850 S).

The hydrogenation of CO_2 was carried out at atmospheric pressure in the temperature range 150–300 °C. The total flow rate used in the experiments, which involved a CO_2/H_2 mixture (CO_2/H_2 = 1/9 v/v), was 100 $Ncm^3\ min^{-1}$. Gas effluents were monitored with a micro gas chromatograph (Varian CP-4900) fitted with a PoraPLOT Q column and a molecular sieve column, each of which was connected to a thermal conductivity detector (TCD). All catalytic tests were performed twice and the relative error was less than 5%.

Catalytic parameters were calculated as follows (Eq. (5)–(7)):

$$Formation\ rate_i(\mu mol \cdot min^{-1} \cdot g^{-1}) = \frac{F_i}{Catalyst\ weight} \quad (5)$$

$$Selectivity_i(\%) = \frac{F_i}{F^0_{CO_2} - F_{CO_2}} \times 100 \quad (6)$$

$$CO_2\ conversion(\%) = \frac{F^0_{CO_2} - F_{CO_2}}{F^0_{CO_2}} \times 100 \quad (7)$$

where F_i represents the molar flow (μmol min^{-1}) of the i component (CH_3OH or CO).

3. Results and discussion

3.1. Textural properties

The main textural properties of the support and the prepared catalysts are listed in Table 1 and the corresponding nitrogen adsorption-desorption isotherms are plotted in Fig. 1.

It can be observed that all isotherms corresponded to type II–IV according to the IUPAC classification, and this is characteristic of macroporous and mesoporous materials. A slight volume increase in the middle relative pressure range (0.2–0.5) was observed, whereas a sharp increase took place at high partial pressure (0.8–1) [46,47]. The observed H3-type hysteresis loop (IUPAC classification), which is characteristic of mesoporous materials, is associated with nitrogen capillary condensation [46]. It is worth noting that the shapes of the catalyst isotherms were almost identical to that of the β-SiC support, indicating

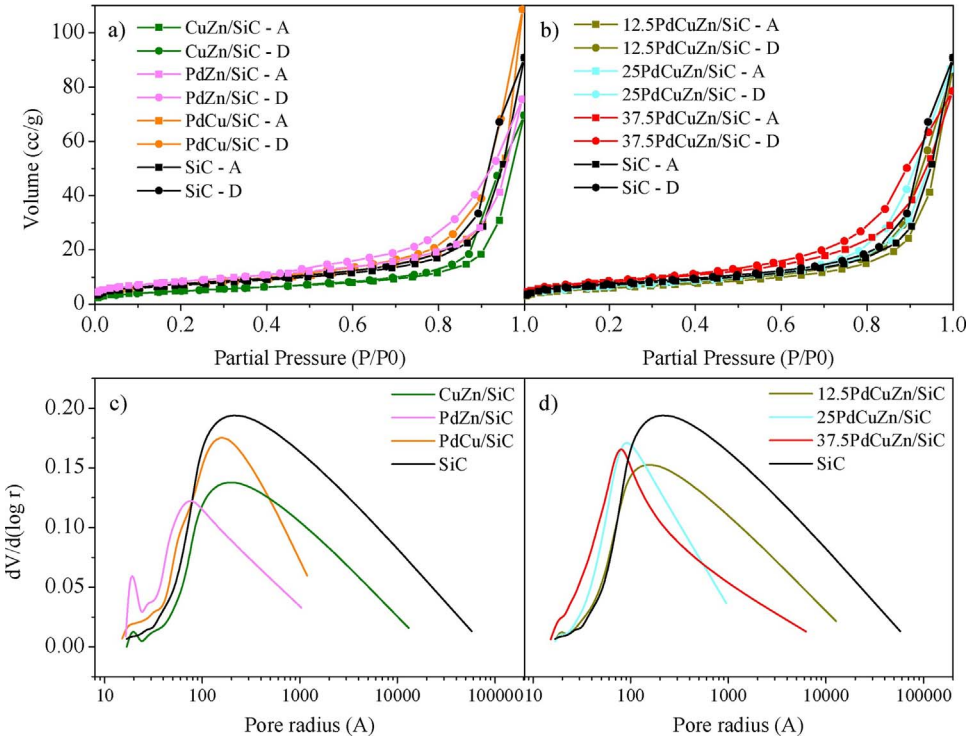

Fig. 1. Nitrogen adsorption–desorption isotherms and mesopore distributions of the support and prepared catalysts.

that the support surface structure did not suffer any significant change after metal incorporation. The variations in the BET surface area, pore volume and average pore radius observed in the catalysts when compared to the support are due to the partial blockage of the β-SiC pores. This blockage is clearly observed in the mesopore distribution of CuZn/SiC (Fig. 1c), which exhibited the same shape as the support but a lower percentage of pores for each radius. Copper particles led to blockage of the pores but the incorporation of palladium led to a decrease in the size of these pores. This behavior can be observed in the mesopore distributions of the trimetallic catalysts (Fig. 1d), where it can be seen that the higher the quantity of palladium, the smaller the pore size. This fact suggests that the presence of Pd led to the formation of smaller metal particles, which partially blocked the pores and thus created smaller ones.

3.2. Metal reducibility

TPR experiments (Fig. 2) were conducted in order to identify an appropriate reduction temperature for all of the catalysts. The results of the TPR analyses for bimetallic catalysts are shown in Fig. 2a. Firstly, CuZn/SiC analysis gave rise to a single broad peak at around 200 °C, which was assigned to the combination of the reduction of Cu^{2+} to Cu^{1+} and Cu^{1+} to Cu^{00} [21]. Moreover, a small broad peak was observed between 450 °C and 680 °C, which can be attributed to ZnO reduction. The PdCu/SiC profile showed a peak at around 50 °C with a shoulder at 90 °C, which was caused by the combination of the reduction of PdO to metallic Pd and the reduction of copper (CuO to Cu^{00}). Therefore, it can be concluded that Pd catalyzed the Cu reduction and

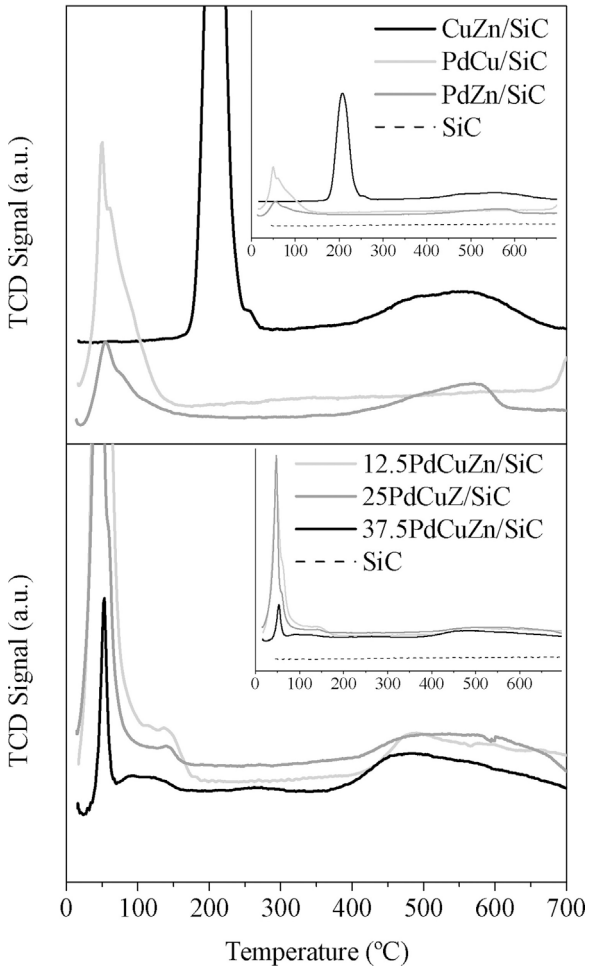

Fig. 2. Temperature-programed reduction (TPR) profiles of (a) bimetallic and (b) trimetallic catalysts.

led to a shift of the corresponding Cu reduction peak to lower temperatures. Finally, PdZn/SiC showed a small peak at around 55 °C, which was also assigned to the reduction of PdO to metallic palladium [48], as well as broad peaks above 400 °C (similar to those that can be seen more clearly in trimetallic catalysts, Fig. 2b), which are commonly related to crystalline PdZn alloy formation [49–51]. It is important to note that the TPR profile of the support did not show any noticeable peak.

If the amount of hydrogen consumed for these peaks were calculated, only a small proportion of palladium would have been reduced. According to the literature [49,50], hydrogen consumption occurs rapidly when hydrogen is fed over the catalyst at room temperature and PdO is partially converted to PdH_x [48]. These palladium hydrides are then decomposed to metallic palladium [24]. A proper quantification of such changes was not possible to carry out as hydrogen was in contact with the catalyst before the TPR data recording started, so that it was not possible to draw any conclusion concerning this fact.

As the amount of Pd increased, the trimetallic catalyst profiles changed from the CuZn/SiC-type to the PdZn/SiC-type. In this way, the profile for 12.5PdCuZn/SiC showed a broad peak (50 °C) with two shoulders (60 and 140 °C), which are ascribed to Pd ($PdO \rightarrow Pd^{00}$) and Cu ($Cu^{2+} \rightarrow Cu^{+} \rightarrow Cu^{00}$) reduction, respectively. As mentioned above, this finding revealed how palladium catalyzes the reduction of copper particles and thus decreases the temperature of the reduction peak. The 25PdCuZn/SiC profile was similar to that of the bimetallic PdCu/SiC, with the shoulder for the trimetallic catalyst shifted to higher temperatures due to the lower amount of Pd. Finally, the 37.5PdCuZn/SiC sample showed a pattern similar to that of PdZn/SiC. All of the trimetallic catalysts showed different broad peaks above 400 °C and these could be related to the formation of PdZn alloy during the reduction process [52], in a similar way to PdZn/SiC.

Bearing in mind the TPR results, 500 °C was selected as an appropriate reduction temperature to ensure the complete reduction of all metals and the formation of the PdZn alloy, which is an active phase for methanol formation [22,24]. It is worth noting that the β-SiC structure remained unchanged at this temperature, since this material did not show any appreciable peak in the temperature range studied.

3.3. Crystalline structure and active metal phases

The X-ray diffractograms of reduced bimetallic and trimetallic catalysts are shown in Fig. 3. On the one hand, the diffractograms of bimetallic catalysts contain the main peaks related to the metallic phases or alloys formed, as well as those attributed to the β-SiC (JPCDS 02-1050). Hence, the CuZn/SiC diffractogram showed the metallic cubic copper crystal structure (JPCDS 85-1326), whereas the PdZn/SiC diffractogram contained the peaks of the PdZn alloy (JPCDS 06-0620). Finally, the PdCu/SiC diffractogram showed the peaks related to PdCu alloy (JPCDS 48-1551) along with those of metallic copper. The presence of ZnO in all of the catalysts prepared with zinc was expected but the main diffraction peak at 2θ = 36.2° (JCPDS 80-0075) was hidden by those of β-SiC.

The peak identification was more difficult in the case of trimetallic catalysts as it was expected that some diffraction peaks would overlap. Although it could be asserted that 12.5PdCuZn/SiC contained metallic copper particles in its structure, the other peak at around 41° could correspond to PdZn, PdCu or both alloys, the main diffraction peaks of which appear at similar values (2θ–41.2° and 41.4°), respectively. The same problem was found in the diffractograms of 25PdCuZn/SiC and 37.5PdCuZn/SiC, for which it was not possible to identify the broad peak and its shoulder observed between 2θ = 40° and 45°. Even if the identification were easier, the peak could shift respect its corresponding 2θ value, which would indicate the formation of alloys as observed in other metal configurations [53,54]. Nevertheless, it was not possible to conclude anything from XRD results. Finally, although diffraction peaks of Pd^0 were expected, the high reflections of β-SiC along with the high

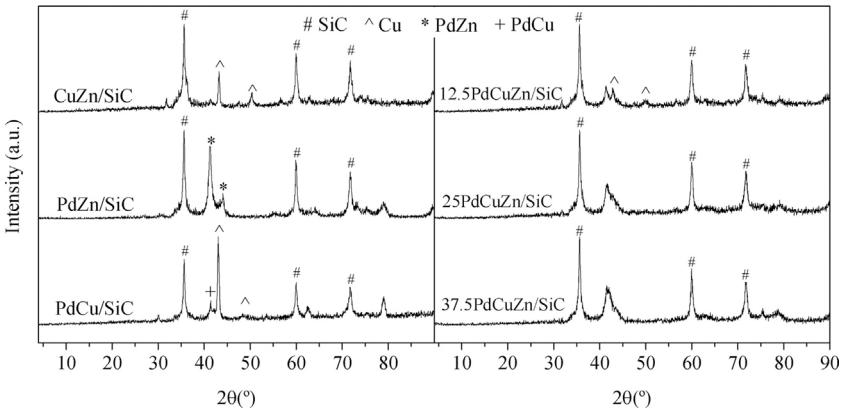

Fig. 3. XRD profiles of the reduced catalysts.

dispersion of this metal made impossible any identification.

The particle size diameters obtained by XRD, which were calculated from the main diffraction peaks of the corresponding compounds, are listed in Table 1. The results are consistent with the N_2 adsorption/desorption results. On the one hand, larger metal particles, which blocked the pores of the support, were expected for CuZn/SiC and PdCu/SiC. On the other hand, smaller metal particles were found as the palladium content increased in trimetallic catalysts. These smaller metal particles partially blocked the β-silicon carbide pores, thus decreasing their size. It is important to note that the average particle sizes for 25PdCuZn/SiC and 37.5PdCuZn/SiC were lower than that of PdZn/SiC, which suggests that a synergistic effect occurs between metals and this leads to smaller particles.

To gain an insight into the compounds formed on the surface of the support, TEM and EDX analyses were carried out on various regions of the reduced catalysts. As an example, representative results are shown in Fig. 4 and Table 2, respectively. All catalysts exhibited a Gaussian particle size distribution and the mean particle sizes evaluated by TEM are consistent with those obtained by XRD (Table 1). The smallest particles were found in trimetallic 37.5PdCuZn/SiC. Energy dispersive X-ray (EDX) microanalysis results revealed that, regardless of the percentage of copper, the particles of both trimetallic catalysts contained a high level of this metal in their structure. The differences in metal percentages between the other metals (Pd and Zn) confirmed a higher percentage of palladium in 37.5PdCuZn/SiC. As for PdZn/SiC, it was observed in all cases a Pd/Zn ratio higher than 1 (1.25 in Region B), which suggested, in agreement with XRD results, the formation of PdZn and Pd^0 phases during reduction.

Bearing in mind the characterization results obtained to this point, it is possible to suggest a theory regarding the active phases formed in each sample during reduction (Fig. 5). On the one hand, the active phases of bimetallic catalysts should be those expected from XRD – with the exception of PdZn/SiC, for which the smallest particles found in the particle size distribution (< 5 nm, Fig. 4d) are probably related to metallic palladium, since this noble metal is known to disperse well. On the other hand, the formation of the active phases is more complex in trimetallic catalysts. According to the representative EDX results listed in Table 2, in which the atomic percentage of Cu was far higher than those of Pd and Zn, the first metal that is deposited on the support is copper, followed by palladium and zinc, which are deposited to form the PdZn alloy observed by XRD (Fig. 3). In addition, the remaining palladium is likely to form an alloy (PdCu) with the copper on which it is deposited. Finally, due to the higher percentage of copper impregnated in 12.5PdCuZn/SiC, isolated copper metal particles are deposited, as also observed by XRD (Fig. 3). Outside the regions marked in Fig. 4, isolated ZnO was expected to deposit because of the higher percentage of this compound. This fact was confirmed by XPS spectra, which also provided valuable information that supported the theory outlined above (see hereafter).

3.4. Metal surface structures

To gain a more in-depth knowledge of the metal surface structures formed in the catalysts and detect the presence of potential alloys, the chemical state and the relative surface abundance of copper, palladium and zinc were evaluated by X-ray photoelectron spectroscopy (XPS). The Cu 2p, Pd 3d and Zn 2p XPS spectra for the bimetallic and trimetallic catalysts are shown in Fig. 6 and the binding energies and the atomic ratios of all elements are listed in Table 3.

The Cu 2p spectra showed a single peak at around 932 eV, which corresponds to the $2p_{3/2}$ value of metallic copper. As expected, in trimetallic catalysts the lower the amount of copper, the lower the intensity of the peak. On the other hand, the low atomic ratios of Cu/Zn and Cu/Pd demonstrate that copper was not deposited efficiently on the surface, with levels that are practically negligible in CuZn/SiC and 37.5PdCuZn/SiC. These findings confirm the theory proposed above (Fig. 5).

As far as the Pd 3d spectra are concerned, the $3d_{5/2}$ binding energies of the peaks observed in trimetallic samples were similar to those reported in the literature for the PdZn alloy (336 eV) [55]. The $3d_{5/2}$ peak of PdZn/SiC was shifted to lower values and this confirmed the presence of metallic palladium (335 eV) on the surface of the catalyst. This fact was corroborated by quantification of the Pd/Zn atomic ratios (Table 3), with a value higher than one obtained for PdZn/SiC. In contrast, the value for 37.5PdCuZn/SiC was close to one. Finally, the PdCu/SiC sample also gave the $3d_{5/2}$ peak in the binding energy of metallic palladium (335 eV). In contrast to PdZn, it has been reported in previous studies [25,56] that the Pd 3d doublet of the bulk PdCu alloy did not show any peak shift with respect to the pure metal.

Finally, three different profiles were observed in the Zn 2p spectra. CuZn/SiC and 12.5PdCuZn/SiC showed a peak at 1023 eV, which corresponds to the $2p_{3/2}$ level of zinc oxide. As to PdZn/SiC, this peak was shifted to lower binding energies, thus confirming that all of the surface zinc was used to form the PdZn alloy. The case of 37.5PdCuZn/SiC warrants a special mention as the $2p_{3/2}$ peak maximum appeared between the values of ZnO and Zn^0. In this catalyst, although Pd and Zn also interacted to form a PdZn alloy, the initial amount of Pd introduced was lower than that of Zn and the remaining ZnO was observed in the spectrum. For this reason, in the interpretation of the species distribution in the catalyst surface (Fig. 5) it was expected that the ZnO would be present in trimetallic catalysts. In brief, the XPS results support the theory proposed and are consistent with the results of the characterization techniques described above.

3.5. Catalytic activity

The catalytic performance of bimetallic and trimetallic catalysts is shown in Fig. 7. On the one hand, it can be observed that a higher reaction temperature led to a higher formation rate of carbon monoxide

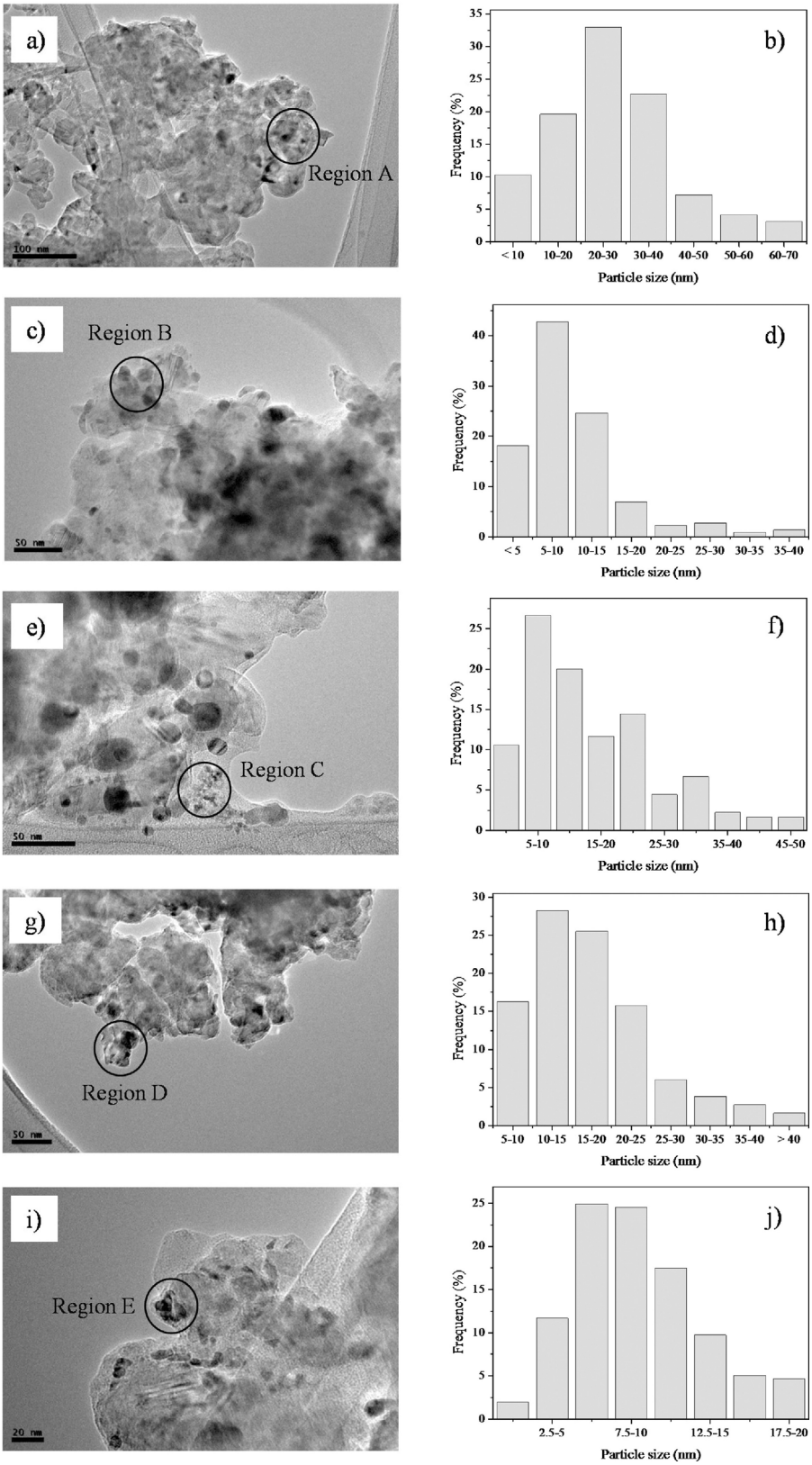

Fig. 4. TEM images and metal particle distribution of (a, b) CuZn/SiC; (c, d) PdZn/SiC; (e, f) PdCu/SiC; (g, h) 12.5PdCuZn/SiC and (i, j) 37.5PdCuZn/SiC samples.

(Fig. 7a). The PdZn/SiC catalyst showed the highest CO formation rate by the reverse water-gas-shift reaction (RWGS, eq. 3), closely followed by CuZn/SiC, whereas the behavior of the bimetallic PdCu/SiC was similar to that observed for trimetallic catalysts. The curves for the methanol formation rate were different to those for carbon monoxide (Fig. 7b), with a maximum value observed between 225 and 275 °C depending on the catalyst. PdCu/SiC did not show any activity towards methanol and this indicates that the PdCu alloy observed in this catalyst was not active for methanol production at atmospheric pressure – in contrast to the situation reported for high pressure conditions (4.1 MPa), where the PdCu alloy was selective to methanol [25]. The methanol formation rate for trimetallic catalysts increased as the

Table 2
Energy dispersive X-ray microanalysis results of regions from Fig. 4.

	Atomic%				
Element	Region A	Region B	Region C	Region D	Region E
Cu	78.7	–	68	74.3	62.8
Pd	–	55.5	32	5.9	18.9
Zn	21.3	44.5	–	19.8	18.3

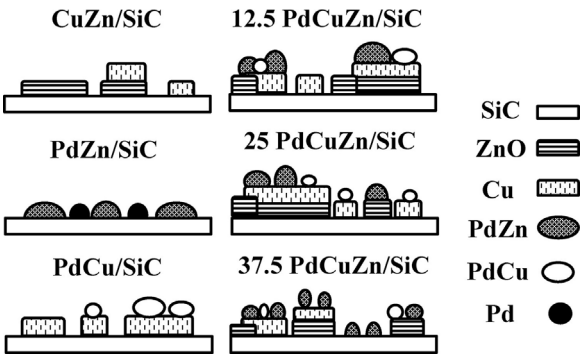

Fig. 5. Proposed theory for active phase formation during reduction.

palladium loading increased, and the curves varied from the CuZn/SiC-type profile, whose activity to methanol was limited, to the PdZn/SiC-type profile, in which the PdZn alloy played an important role in methanol formation [24,44]. Interestingly, the methanol formation rate for 37.5PdCuZn/SiC was higher at 250 and 275 °C than that for PdZn/SiC, which revealed that the combination of Pd-Cu-Zn improved the catalytic performance towards methanol synthesis. This attractive behavior was observed more clearly in the selectivity towards methanol (Fig. 7c), where the trimetallic catalyst showed the highest values over the whole range of temperatures studied. Indeed, the values obtained with 12.5PdCuZn/SiC, in which only a low level of palladium was deposited, were higher than those for PdZn/SiC and CuZn/SiC. This finding also underlines the synergistic effect produced by the combination of Pd, Cu and Zn. Finally, the CO_2 conversion curves (Fig. 7d) showed a similar trend to the CO formation rate curves, since these species were the predominant products at high temperatures. It should be noted that, even though the catalytic experiments were carried out under atmospheric pressure, the results are far away from the thermodynamic equilibrium values (except at 275 °C) showing that there are not thermodynamic limitations (see Table 4 where the thermodynamic and experimental results for the 37.5PdCuZn/SiC catalyst are compared). The thermodynamic equilibrium values were calculated using a flowsheet simulator (Aspen HYSYS V8.4 licensed by Aspen Technology,Inc.). Peng Robinson was used as the equation of state and the reactor modeling was based on a Gibbs reactor. The conditions used for the simulation (flow rate, CO_2/H_2 ratio) were the same as in the experimental reactor.

The catalytic results can be explained by the theory proposed for the formation of particles on the catalyst surface (Fig. 5). The high CO formation rate observed in PdZn/SiC was probably due to the presence of small particles of metallic palladium, which were observed in the reduced catalyst, and this idea is consistent with previous studies [22,24]. On the other hand, when trimetallic catalysts were reduced, all of the metallic palladium interacted with Zn and Cu to form the corresponding PdZn and PdCu alloys. This new alloy (PdCu) was not as active to carbon monoxide as metallic palladium (Fig. 7a) and it can therefore be concluded that copper acted as an inhibitor of this metal in trimetallic catalysts, which in turn led to a higher selectivity to methanol. Moreover, it can be seen from the catalyst particle diameters (Table 1) that trimetallic 37.5PdCuZn/SiC average particle size was

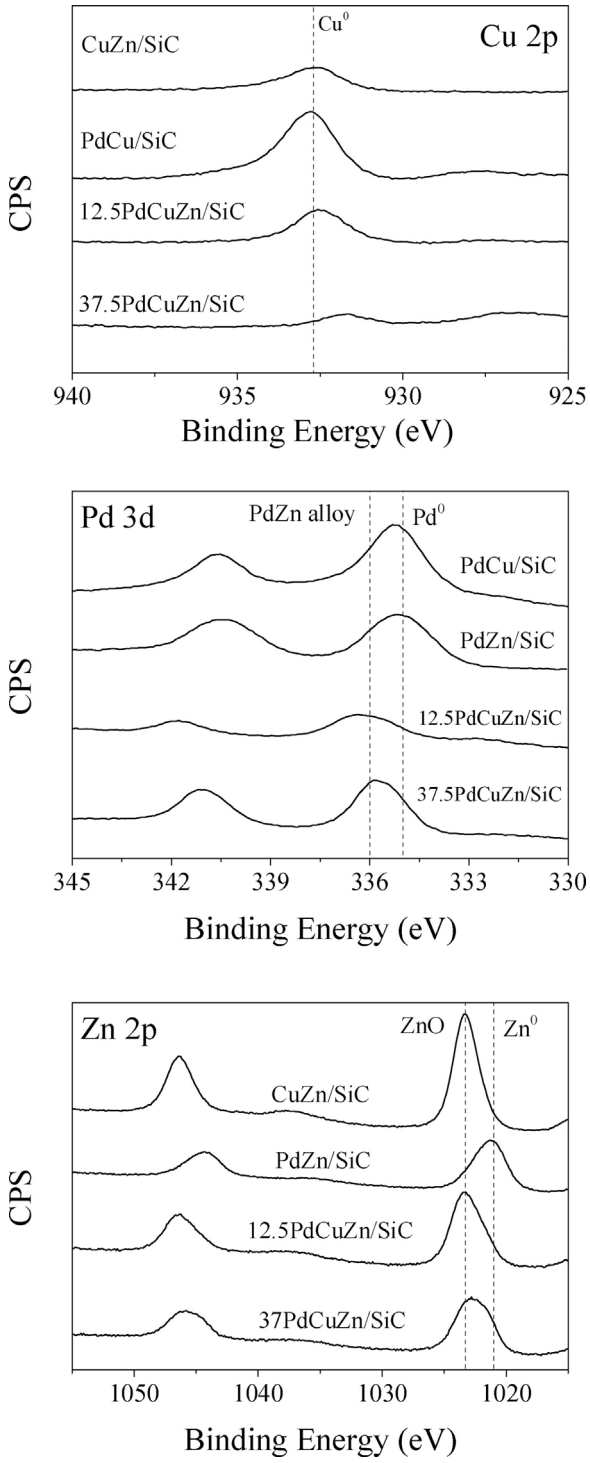

Fig. 6. XPS spectra of reduced catalysts in the Cu 2p, Pd 3d and Zn 2p regions.

Table 3
Binding energies and surface atomic ratios for the bimetallic and tri-metallic catalysts.

	Binding Energies (eV)			Atomic ratio		
Sample	Pd 3d 5/2	Cu 2p 3/2	Zn 2p 3/2	Pd/Zn	Cu/Zn	Cu/Pd
CuZn/SiC	–	932.5	1023.3	–	0.09	–
PdCu/SiC	335.3	932.8	–	–	–	0.16
PdZn/SiC	335.1	–	1021.3	2.04	–	–
12.5PdCuZn/SiC	336.1	932.6	1023.2	0.71	0.15	0.21
37.5PdCuZn/SiC	335.7	931.8	1022.8	1.18	0.07	0.06

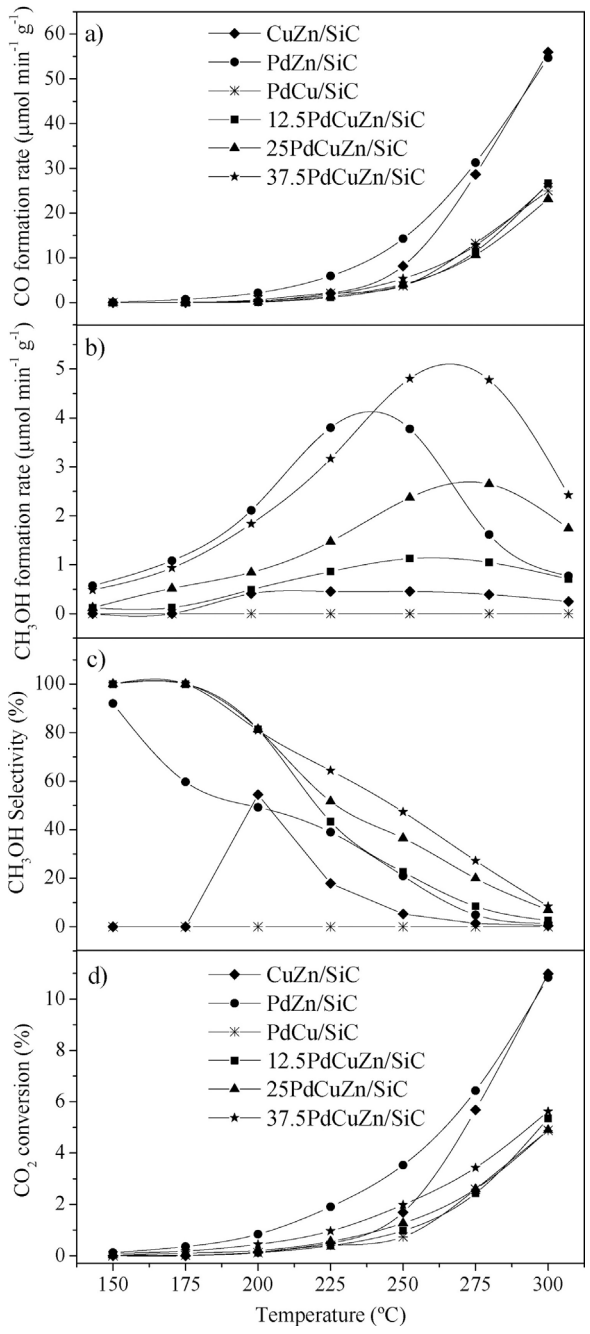

Fig. 7. Catalytic activity of bimetallic and trimetallic catalysts. Reaction conditions: CO_2/H_2 = 1/9 (v/v) and W/F = 0.008 g min cm^{-3}.

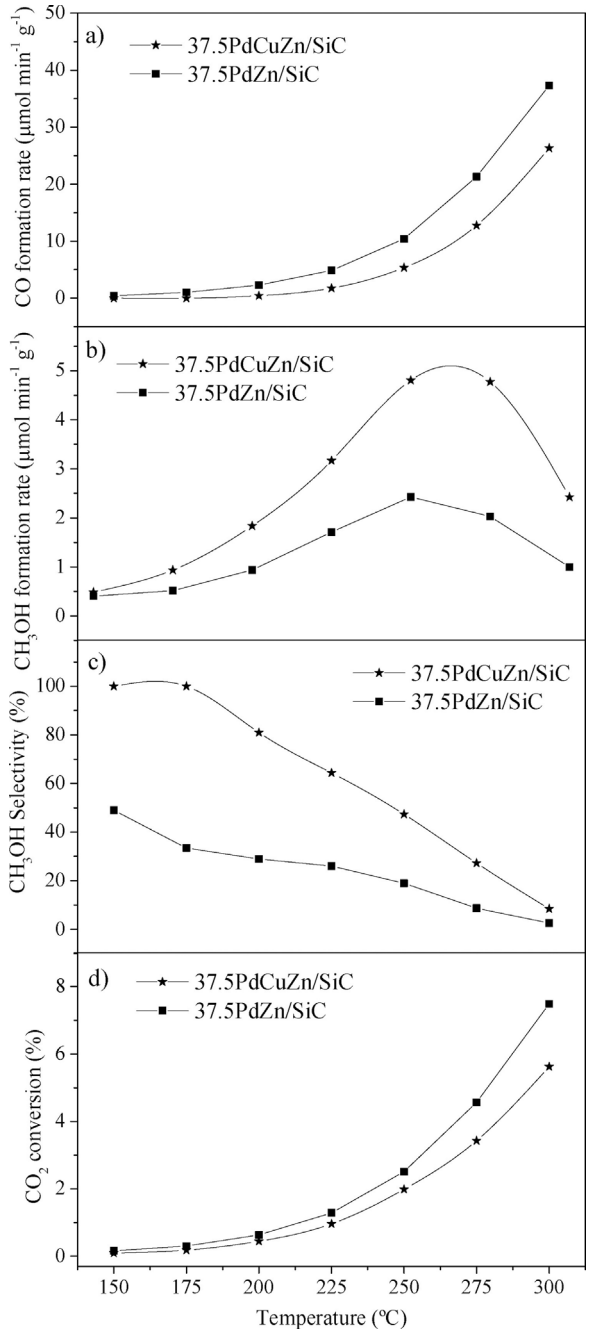

Fig. 8. Comparison between the catalytic activity of 37.5PdCuZn/SiC and 37.5PdZn/SiC. Reaction conditions: CO_2/H_2 = 1/9 (v/v) and W/F = 0.008 g min cm^{-3}.

Table 4
Comparison between thermodynamic equilibrium and experimental values for the catalyst 37.5PdCuZn/SiC.

Temperature (°C)	Thermodynamic (μmol/min)	Experimental (μmol/min)
150	22.24	0.39
175	14.72	0.75
200	10.09	1.47
225	7.14	2.53
250	5.19	3.85
275	3.87	3.82
300	2.95	1.94

lower than that of bimetallic PdZn/SiC. Therefore, the metal particles were better dispersed in the trimetallic catalyst, probably due to a synergistic effect between the metals. The higher methanol formation rate obtained on using 37.5PdCuZn/SiC could be explained by taking into account two facts: (i) The PdZn alloy particles of this catalyst were smaller and better dispersed than those of bimetallic PdZn/SiC, and (ii) once the metallic palladium had been transformed into PdCu alloy, which was observed to be less active towards CO formation than metallic palladium, the reactant molecules (H_2 and CO_2) were prone to react on the PdZn active sites, thus leading to a higher methanol formation rate.

In an effort to demonstrate that the presence of copper is necessary to obtain a catalyst that is more active and selective to methanol than

Table 5
Comparison of the 37.5PdCuZn/SiC catalytic performance with the literature.

Sample	Reaction conditions		Methanol catalytic performance		Reference
	Temperature (°C)	CO_2/H_2 (v/v)	Activity (μmol g^{-1} min^{-1})	Selectivity (%)	
37.5PdCuZn/SiC	200	1/9	1.84	80.9	This work
Pd/ZnO	190	1/9	1.28	65.1	[37]
Cu/ZnO	190	1/9	1.74	30.4	[37]

the PdZn/SiC catalyst, a new PdZn/SiC catalyst (37.5PdZn/SiC) was prepared with molar percentages of 37.5% and 62.5% for palladium and zinc, respectively. The results for comparison with the corresponding trimetallic catalyst (37.5PdCuZn/SiC) are shown in Fig. 8. It was observed that the activities to methanol and CO of 37.5PdZn/SiC were lower and higher, respectively, than those of 37.5PdCuZn/SiC. These results support the situation described above in that the activity of 37.5PdZn/SiC to CO was higher because, in the absence of copper, particles of metallic palladium that led to CO production remained on the catalyst. At the same time, the activity to CH_3OH decreased due to the high activity of these metallic palladium active sites, which led to competition between them and the PdZn sites to adsorb H_2 and CO_2. Therefore, the contribution of copper in trimetallic 37.5PdCuZn/SiC proved to be crucial.

Finally, the catalytic performance of 37.5PdCuZn/SiC was compared to the results reported by Iwasa et al. [44], which to the best of our knowledge is the only study on CO_2 hydrogenation at atmospheric pressure with palladium zinc catalysts (Table 5). Despite the differences between the catalysts (metal loading, morphology) and the reaction conditions (463 vs 473 K), it can be asserted that trimetallic 37.5PdCuZn/SiC was more active and, in particular, selective towards methanol than Pd/ZnO or Cu/ZnO.

In conclusion, the aim of this work was achieved and the trimetallic catalyst 37.5PdCuZn/SiC proved to be more active and selective to methanol than the bimetallic PdZn/SiC one. The synergistic effect between Pd-Cu-Zn is responsible for this promising behavior.

4. Conclusions

The following conclusions can be drawn from this study:

- Cu, Pd and Zn exhibited a synergistic effect in trimetallic catalysts. On the one hand, Pd interacted with Zn and Cu to form the corresponding PdZn and PdCu alloys, which were selective towards methanol and CO, respectively. On the other hand, the average metal particle size was generally lower than that of the corresponding bimetallic catalysts.
- TEM and XPS analyses of trimetallic catalysts suggest that, during the reduction process, ZnO and Cu were the first compounds deposited onto the SiC support and the alloys of PdZn and PdCu were then formed on top.
- Cu acted as an inhibitor of metallic palladium through the formation of the PdCu alloy, which was less active towards CO than Pd^0.
- The combination of PdZn and PdCu active sites led to highly methanol-selective trimetallic catalysts.
- An optimum trimetallic catalyst (37.5PdCuZn/SiC) was selected as the best example as it showed the highest methanol formation rate. Hence, an optimization of the composition of the trimetallic catalysts was performed, which was of crucial interest because of the high price of palladium.

Acknowledgments

The authors would like to thank the Ministerio de Economía y Competitividad (Project No. PCIN-2013-183), the Spanish government (grant FPU13/00727) and the University of Castilla – La Mancha (Energy and environment talent program – E2TP) for their financial support.

References

[1] H. Harde, Scrutinizing the carbon cycle and CO_2 residence time in the atmosphere, Global Planet. Change 152 (2017) 19–26.
[2] J.C.A. Pistevos, I. Nagelkerken, T. Rossi, S.D. Connell, Ocean acidification alters temperature and salinity preferences in larval fish, Oecologia 183 (2017) 545–553.
[3] W.D. Nordhaus, Revisiting the social cost of carbon, Proc. Nat. Acad. Sci. U. S. A. 114 (2017) 1518–1523.
[4] P. Villoria-Sáez, V.W.Y. Tam, M.D. Río Merino, C. Viñas Arrebola, X. Wang, Effectiveness of greenhouse-gas Emission Trading Schemes implementation: a review on legislations, J. Clean. Prod. 127 (2016) 49–58.
[5] P.A. Alaba, A. Abbas, W.M.W. Daud, Insight into catalytic reduction of CO_2: Catalysis and reactor design, J. Clean. Prod. 140 (2017) 1298–1312.
[6] S. Saeidi, N.A.S. Amin, M.R. Rahimpour, Hydrogenation of CO_2 to value-added products − A review and potential future developments, J. CO_2 Util. 5 (2014) 66–81.
[7] I. Ganesh, Conversion of carbon dioxide into methanol – A potential liquid fuel: fundamental challenges and opportunities (a review), Renew. Sust. Energ. Rev. 31 (2014) 221–257.
[8] A.A. Olajire, Valorization of greenhouse carbon dioxide emissions into value-added products by catalytic processes, J. CO_2 Util. 3-4 (2013) 74–92.
[9] N. Gutiérrez-Guerra, L. Moreno-López, J.C. Serrano-Ruiz, J.L. Valverde, A. de Lucas-Consuegra, Gas phase electrocatalytic conversion of CO_2 to syn-fuels on Cu based catalysts-electrodes, Appl. Catal. B-Environ. 188 (2016) 272–282.
[10] K.A. Ali, A.Z. Abdullah, A.R. Mohamed, Recent development in catalytic technologies for methanol synthesis from renewable sources: a critical review, Renew. Sust. Energ. Rev. 44 (2015) 505–518.
[11] G.A. Olah, Beyond oil and gas the methanol economy, Angew. Chem. Int. Ed. 44 (2005) 2636–2639.
[12] S.G. Jadhav, P.D. Vaidya, B.M. Bhanage, J.B. Joshi, Catalytic carbon dioxide hydrogenation to methanol: a review of recent studies, Chem. Eng. Res. Des. 92 (2014) 2557–2567.
[13] J. Sloczynski, R. Grabowski, A. Kozlowska, P. Olszewski, J. Stoch, J. Skrzypek, M. Lachowska, Catalytic activity of the M/(3ZnO·ZrO_2) system (M = Cu, Ag Au) in the hydrogenation of CO_2 to methanol, Appl. Catal. A-Gen. 278 (2004) 11–23.
[14] G.G. Asara, J.M. Ricart, J.A. Rodriguez, F. Illas, Exploring the activity of a novel Au/TiC (001) model catalyst towards CO and CO_2 hydrogenation, Surf. Sci. 640 (2015) 141–149.
[15] A. Vourros, I. Garagounis, V. Kyriakou, S.A.C. Carabineiro, F.J. Maldonado-Hódar, G.E. Marnellos, M. Konsolakis, Carbon hydrogenation over supported Au nanoparticles: effect of the support, J. CO_2 Util. 19 (2017) 247–256.
[16] R. Grabowski, J. Sloczynski, M. Sliwa, D. Mucha, R.P. Socha, Influence of polymorphic ZrO_2 phases and the silver electronic state on the activity of Ag/ZrO_2 catalysts in the hydrogenation of CO_2 to methanol, ACS Catal. 1 (2011) 266–278.
[17] P. Reyes, I. Concha, G. Pecchi, J.L.G. Fierro, Changes induced by metal oxide promoters in the performance of Rh-Mo/ZrO_2 catalysts during CO and CO_2 hydrogenation, J. Mol. Catal. A: Chem. 129 (1998) 269–278.
[18] H. Ahouari, A. Soualah, A. Le Valant, L. Pinard, P. Magnoux, Y. Pouilloux, Methanol synthesis from CO_2 hydrogenation over copper based catalysts, React. Kinet. Mech. Cat. 110 (2013) 131–145.
[19] E.L. Kunkes, F. Studt, F. Abild-Pedersen, R. Schlögl, M. Behrens, Hydrogenation of CO_2 to methanol and CO on Cu/ZnO/Al_2O_3: Is there a common intermediate or not? J. Catal. 328 (2015) 43–48.
[20] G. Wang, L. Chen, Y. Sun, J. Wu, M. Fu, D. Ye, Carbon dioxide hydrogenation to methanol over Cu/ZrO_2/CNTs: effect of carbon surface chemistry, RSC Adv. 5 (2015) 45320–45330.
[21] J. Díez-Ramírez, F. Dorado, A.R. de la Osa, J.L. Valverde, P. Sánchez, Hydrogenation of CO_2 to methanol at atmospheric pressure over Cu/ZnO catalysts: influence of the calcination, reduction, and metal loading, Ind. Eng. Chem. Res. 56 (2017) 1979–1987.
[22] J. Díez-Ramírez, P. Sánchez, A. Rodríguez-Gómez, J.L. Valverde, F. Dorado, Carbon nanofiber-based palladium/zinc catalysts for the hydrogenation of carbon dioxide to methanol at atmospheric pressure, Ind. Eng. Chem. Res. 55 (2016) 3556–3567.
[23] J. Díez-Ramírez, P. Sánchez, J.L. Valverde, F. Dorado, Electrochemical promotion and characterization of PdZn alloy catalysts with K and Na ionic conductors for pure gaseous CO_2 hydrogenation, J. CO_2 Util. 16 (2016) 375–383.
[24] J. Díez-Ramírez, J.L. Valverde, P. Sánchez, F. Dorado, CO_2 hydrogenation to methanol at atmospheric pressure: influence of the preparation method of Pd/ZnO

Catalysts, Catal. Lett. 146 (2016) 373–382.
[25] X. Jiang, N. Koizumi, X. Guo, C. Song, Bimetallic Pd-Cu catalysts for selective CO_2 hydrogenation to methanol, Appl. Catal. B-Environ. 170–171 (2015) 173–185.
[26] I. Melián-Cabrera, M. López Granados, P. Terreros, J.L.G. Fierro, CO_2 hydrogenation over Pd-modified methanol synthesis catalysts, Catal. Today 45 (1998) 251–256.
[27] I. Melián-Cabrera, M.L. Granados, J.L.G. Fierro, Effect of Pd on Cu-Zn catalysts for the hydrogenation of CO_2 to methanol: stabilization of Cu metal against CO_2 oxidation, Catal. Lett. 79 (2002) 165–170.
[28] M. Sahibzada, D. Chadwick, I.S. Metcalfe, Hydrogenation of carbon dioxide to methanol over palladium-promoted $Cu/ZnO/Al_2O_3$ catalysts, Catal. Today 29 (1996) 367–372.
[29] K. Siriworarat, V. Deerattrakul, P. Dittanet, P. Kongkachuichay, Production of methanol from carbon dioxide using palladium-copper-zinc loaded on MCM-41: Comparison of catalysts synthesized from flame spray pyrolysis and sol-gel method using silica source from rice husk ash, J. Clean. Prod. 142 (2017) 1234–1243.
[30] P. Mierczynski, R. Ciesielski, A. Kedziora, O. Shtyka, T.P. Maniecki, Methanol synthesis using copper catalysts supported on CeO_2-Al_2O_3 mixed oxide, Fibre Chem. 48 (2017) 271–275.
[31] X.K. Phan, J.C. Walmsley, H. Bakhtiary-Davijany, R. Myrstad, P. Pfeifer, H. Venvik, A. Holmen, Pd/CeO_2 catalysts as powder in a fixed-bed reactor and as coating in a stacked foil microreactor for the methanol synthesis, Catal. Today 273 (2016) 25–33.
[32] T. Phongamwong, U. Chantaprasertporn, T. Witoon, T. Numpilai, Y. Poo-arporn, W. Limphirat, W. Donphai, P. Dittanet, M. Chareonpanich, J. Limtrakul, CO_2 hydrogenation to methanol over CuO–ZnO–ZrO_2–SiO_2 catalysts: effects of SiO_2 contents, Chem. Eng. J. 316 (2017) 692–703.
[33] K. Larmier, W.C. Liao, S. Tada, E. Lam, R. Verel, A. Bansode, A. Urakawa, A. Comas-Vives, C. Copéret, CO_2-to-methanol hydrogenation on zirconia-supported copper nanoparticles: reaction intermediates and the role of the metal–support interface, Angew. Chem. Int. Ed. 56 (2017) 2318–2323.
[34] X. Dong, H.-B. Zhang, G.-D. Lin, Y.-Z. Yuan, K.R. Tsai, Highly active CNT-promoted Cu–ZnO–Al_2O_3 catalyst for methanol synthesis from $H_2/CO/CO_2$, Catal. Lett. 85 (2003) 237–246.
[35] J. Díez-Ramírez, P. Sánchez, V. Kyriakou, S. Zafeiratos, G.E. Marnellos, M. Konsolakis, F. Dorado, Effect of support nature on the cobalt-catalyzed CO_2 hydrogenation, J. CO_2 Util. 21 (2017) 562–571.
[36] G. Bonura, M. Cordaro, C. Cannilla, F. Arena, F. Frusteri, The changing nature of the active site of Cu-Zn-Zr catalysts for the CO_2 hydrogenation reaction to methanol, Appl. Catal. B-Environ. 152–153 (2014) 152–161.
[37] N.S.A. Halim, N.A.M. Zabidi, S.F.H. Tasfy, M.S. Shaharun, Morphology and performance of Cu/ZnO based catalyst: comparison between Al_2O_3 and SiC support, AIP Conf. Proc. (2016).
[38] J.M. García-Vargas, J.L. Valverde, J. Díez, P. Sánchez, F. Dorado, Influence of alkaline and alkaline-earth cocations on the performance of Ni/β-SiC catalysts in the methane tri-reforming reaction, Appl. Catal. B-Environ. 148–149 (2014) 322–329.
[39] J.M. García-Vargas, J.L. Valverde, J. Díez, P. Sánchez, F. Dorado, Preparation of Ni-Mg/β-SiC catalysts for the methane tri-reforming: effect of the order of metal impregnation, Appl. Catal. B-Environ. 164 (2015) 316–323.
[40] J.M. García-Vargas, J.L. Valverde, J. Díez, F. Dorado, P. Sánchez, Catalytic and kinetic analysis of the methane tri-reforming over a Ni-Mg/β-SiC catalyst, Int. J. Hydrogen Energ. 40 (2015) 8677–8687.
[41] J.A. Díaz, M. Calvo-Serrano, A.R. De La Osa, A.M. García-Minguillán, A. Romero, A. Giroir-Fendler, J.L. Valverde, í-Silicon carbide as a catalyst support in the fischer-tropsch synthesis: influence of the modification of the support by a pore agent and acidic treatment, Appl. Catal. A-Gen. 475 (2014) 82–89.
[42] J. Zou, X. Mu, W. Zhao, P. Rukundo, Z.J. Wang, Improved catalytic activity of SiC supported Ni catalysts for CO_2 reforming of methane via surface functionalizations, Catal. Commun. 84 (2016) 116–119.
[43] J. Li, J. Wang, D. Gao, X. Li, S. Miao, G. Wang, X. Bao, Silicon carbide-supported iron nanoparticles encapsulated in nitrogen-doped carbon for oxygen reduction reaction, Catal. Sci. Technol. 6 (2016) 2–2954.
[44] N. Iwasa, H. Suzuki, Masao Terashita, M. Arai, N. Takezawa, Methanol synthesis from CO_2 under atmospheric pressure over supported Pd catalysts, Catal. Lett. 96 (2004) 75–78.
[45] T.P. Maniecki, P. Mierczynski, W. Maniukiewicz, K. Bawolak, D. Gebauer, W.K. Jozwiak, Bimetallic Au-Cu, Ag-Cu/$CrAl_3O_6$ catalysts for methanol synthesis, Catal. Lett. 130 (2009) 481–488.
[46] K.S.W. Sing, Reporting Physisorption Data For Gas/Solid Systems, (1984), pp. 567–583.
[47] J.A. Díaz, H. Akhavan, A. Romero, A.M. Garcia-Minguillan, R. Romero, A. Giroir-Fendler, J.L. Valverde, Cobalt and iron supported on carbon nanofibers as catalysts for Fischer-Tropsch synthesis, Fuel Process. Technol. 128 (2014) 417–424.
[48] Y.H. Chin, R. Dagle, J. Hu, A.C. Dohnalkova, Y. Wang, Steam reforming of methanol over highly active Pd/ZnO catalyst, Catal. Today. 77 (2002) 79–88.
[49] N. Iwasa, T. Mayanagi, N. Ogawa, K. Sakata, N. Takezawa, New catalytic functions of Pd-Zn, Pd-Ga Pd-In, Pt-Zn, Pt-Ga and Pt-in alloys in the conversions of methanol, Catal. Lett. 54 (1998) 119–123.
[50] N. Iwasa, S. Masuda, N. Ogawa, N. Takezawa, Steam reforming of methanol over Pd/ZnO: Effect of the formation of PdZn alloys upon the reaction, Appl. Catal. A-Gen. 125 (1995) 145–157.
[51] Y.H. Chin, Y. Wang, R.A. Dagle, X.S. Li, Methanol steam reforming over Pd/ZnO: Catalyst preparation and pretreatment studies, Fuel Process. Technol. 83 (2003) 193–201.
[52] Y. Wang, J. Zhang, H. Xu, Interaction between Pd and ZnO during reduction of Pd/ZnO catalyst for steam reforming of methanol to hydrogen, Chinese J. Catal. 27 (2006) 217–222.
[53] E. Antolini, F. Cardellini, Formation of carbon supported PtRu alloys: an XRD analysis, J.Alloys Compd. 315 (2001) 118–122.
[54] K. Hyun, J.H. Lee, C.W. Yoon, Y. Kwon, The effect of platinum based bimetallic electrocatalysts on oxygen reduction reaction of proton exchange membrane fuel cells, Int. J. Electrochem. Sci. 8 (2013) 11752–11767.
[55] H. Bahruji, M. Bowker, G. Hutchings, N. Dimitratos, P. Wells, E. Gibson, W. Jones, C. Brookes, D. Morgan, G. Lalev, Pd/ZnO catalysts for direct CO_2 hydrogenation to methanol, J. Catal. 343 (2016) 133–146.
[56] A. Rochefort, M. Abon, P. Delichère, J.C. Bertolini, Alloying effect on the adsorption properties of Pd50Cu50{111} single crystal surface, Surf. Sci. 294 (1993) 43–52.